ChemElectroChem

Research Article
doi.org/10.1002/celc.202300443

Chemistry Europe
European Chemical Societies Publishing

www.chemelectrochem.org

# Impact of Acetate-Based Hydrogel Electrolyte on Electrical Performance and Stability of Eco-Friendly Supercapacitors

Giovanni Landi,*[a] Luca La Notte,[b] Veronica Granata,[c] Guerino Avallone,[c] Carlo Barone,[c] Giovanni Carapella,[c] Sergio Pagano,[c] Alessandro Lorenzo Palma,[b] Paolo Sdringola,[b] and Giovanni Puglisi[b]

The electrochemical characteristics and stability of hydrogel-based environmentally friendly supercapacitors employing sodium acetate as salt have been investigated. To ensure the overall sustainability of the devices, chitosan (a biomaterial from renewable resources) and activated carbon (derived from coconut shells) have been used as a binder and filler within the electrodes, respectively. Cyclic voltammetry, galvanostatic charge/discharge, and impedance spectroscopy measurements have been performed to compare the electrochemical properties of the fabricated devices. Compared to reference electrolytes containing NaCl, the utilization of sodium acetate exhibited enhancements in energy performance and stability up to 50000 cycles. The most efficient device has been delivered approximately 10.6 Wh/kg of energy at a high-power density of about 3940 W/kg. A comprehensive investigation of the electrochemical performances has been carried out, considering both faradaic and non-faradaic processes as charge storage mechanisms within the devices. A model has been proposed to describe the storage mechanisms and to provide insights into the ageing phenomena observed during the cycling procedure.

## Introduction

The growing energy demand of human activities requires scientific and technological efforts in the investigation of solutions for sustainable energy production and rational usage. Among the energy storage devices, supercapacitors (SCs), also referred to as electrochemical capacitors, exploit the capacitive properties at the interface between a porous electrode with high specific area and an electrolyte solution.[1] The result is a higher power density compared to batteries and a preferential use in applications requiring a rapid charge-discharge process and larger number of cycles.[2,3] The rapid development of connected and smart electronic devices in the context of the Internet of Things (IoT) offers a great market potential for SCs due to their opportunity to be flexible, lightweight, and miniaturized.[4,5] Moreover, the possibility to prepare the components of SCs from sustainable and green materials[6–8] would represent a valuable alternative to the proliferation of electron waste, that a pervasive IoT would generate with adverse effects on humans and the environment.[9] Usually, electrodes for SCs are homogeneous slurries composed of active materials and additives, coated, or printed on a current collector. While the functional material is generally an activated carbon (AC) derived from bio-based feedstocks,[10] the conventional additive is polyvinylidene fluoride (PVDF), a fluoropolymer that acts as a binder. The drawback is the solubility of this polymer in toxic and volatile organic compounds (e.g., N-methyl-2-pyrrolidone (NMP)). For this reason, water-processable binders originating from renewable sources are desirable for a safer and more sustainable fabrication of electrodes.[11,12] Materials like cellulose and its derivatives, alginate, starch, and chitosan, have been successfully applied as binding materials in carbon electrodes for SCs.[13–15] In particular, chitosan, a polysaccharide extracted from crustacean shells, has been employed without negatively affecting SC performance.[16,17] The overall friendliness of SCs is also improved by using water processing for electrolytes. Aqueous electrolytes provide higher ionic conductivity and lower resistance than organic electrolytes.[18,19] However, the evaporation of water in case of non-optimal encapsulation causes precipitation of the electrolytic salts and, consequently, performance degradation.[20] Moreover, it is not possible to implement the devices in flexible applications. An interesting approach to circumvent the above-mentioned issues is the use of gel polymer electrolytes (GPEs) that combine polymer separator and liquid electrolyte in a homogeneous gel phase, allowing more opportunities for structural design and improvement of stability.[21,22] Among them, hydrogels, composed of an aqueous solution swollen within a polymer matrix, are highly desirable because safe, environmentally friendly and low-cost.[23,24] Recently, hydrogel based on gelatin has been

[a] Dr. G. Landi
Department of Energy Efficiency Unit
Portici Research Center, ENEA
Piazzale Enrico Fermi, 1 Località Granatello, 80055 Portici (Italy)
E-mail: giovanni.landi@enea.it

[b] Dr. L. La Notte, Dr. A. L. Palma, Dr. P. Sdringola, Dr. G. Puglisi
Department of Energy Efficiency Unit
Casaccia Research Center, ENEA
Via Anguillarese 301, 00123 Rome (Italy)

[c] Dr. V. Granata, Dr. G. Avallone, Prof. C. Barone, Prof. G. Carapella, Prof. S. Pagano
Physics Department "E.R. Caianiello" University of Salerno,
Via Giovanni Paolo II 132, 84084 Fisciano (Italy)

Supporting information for this article is available on the WWW under https://doi.org/10.1002/celc.202300443

used as an electrolyte in eco-friendly energy storage devices and low-power sensors for IoT applications.[5,25–28]

In this paper, the fabrication of symmetric carbon-based SCs, with natural polymers employed both in the electrode slurry and electrolyte system has been reported. The latter is a hydrogel containing sodium acetate ($CH_3COONa$) as a highly soluble, and widely available salt, and has already demonstrated to be a beneficial aqueous electrolyte for SCs[29,30] but has been applied for the first time within a GPE. The fabricated devices have been fully characterized in terms of electrochemical performance, emphasizing the advantages of employing sodium acetate in comparison to other reference electrolytes based on NaCl. A detailed investigation has been conducted to establish a clear correlation between cycle stability, charge storage mechanisms, and dielectric properties at the electrode/hydrogel interface for various electrolyte types. Additionally, a model of the impedance spectra that describes the charge storage and the ageing mechanisms within the supercapacitors has been developed.

## Results and Discussion

### Electrical properties

The cross-sectional view of the device, revealing a symmetrical sandwich structure in accordance with the layer sequence: PET/Cu-Tape/Graphite ink/Active material/Gel Polymer Electrolyte, is illustrated in Figure 1(a). Scanning Electron Microscopy (SEM) images of the electrode surface, captured at varying magnifications, are presented in Figures 1(b). All the observed electrodes exhibit uniform and compact surfaces, characterized by the absence of substantial voids or micro-cracks. The GPE consists of a blend of gelatin and water-glycerol molecules with $CH_3COONa$ salt. The estimation of the bulk ionic conductivity $\sigma_{DC}$ from the impedance spectra can be found in the supplementary materials. Figure S1(a) reports the impedance spectra measured for various amounts of $CH_3COONa$ salt within the hydrogel. The measurement has been performed on a thin layer of hydrogel having a thickness of $L = 0.2$ cm and an area of 5 $cm^2$. The GPE layer has been in contact with two copper foils. The cross-section of the test structure is shown in the inset of Figure 1(c). In the same figure, ionic conductivity values as a function of the sodium acetate concentration within the hydrogel measured at 300 K are shown. The $\sigma_{DC}$ values of the undoped hydrogel range between 0.4 to 0.7 mS/cm, consistent with findings reported in the literature.[27,31] The incorporation of the $CH_3COONa$ salt into the pristine gelatin blend changes the value of $\sigma_{DC}$. In particular, the ionic conductivity progressively increases, reaching a value of 13.2 mS/cm at 2.5 M, and then gradually decreases to 1.4 mS/cm at 4 M.

This finding highlights the importance of selecting the optimal salt content of 2.5 M to attain the utmost level of ionic conductivity, thereby leading to the optimal performance of the supercapacitor. This is further supported by the phase angle dependence on the frequency, as displayed in Figure S1 (b). Significantly, the GPE containing 2.5 M of $CH_3COONa$ salt exhibits a sustained dielectric response in a higher frequency range compared to the hydrogel with other acetate concentrations. It is worth noting that the ionic conductivity value reported in the literature for the aqueous electrolyte with 2.5 M sodium acetate is approximately 75 mS/cm.[29] The observed decrease in $\sigma_{DC}$ value,

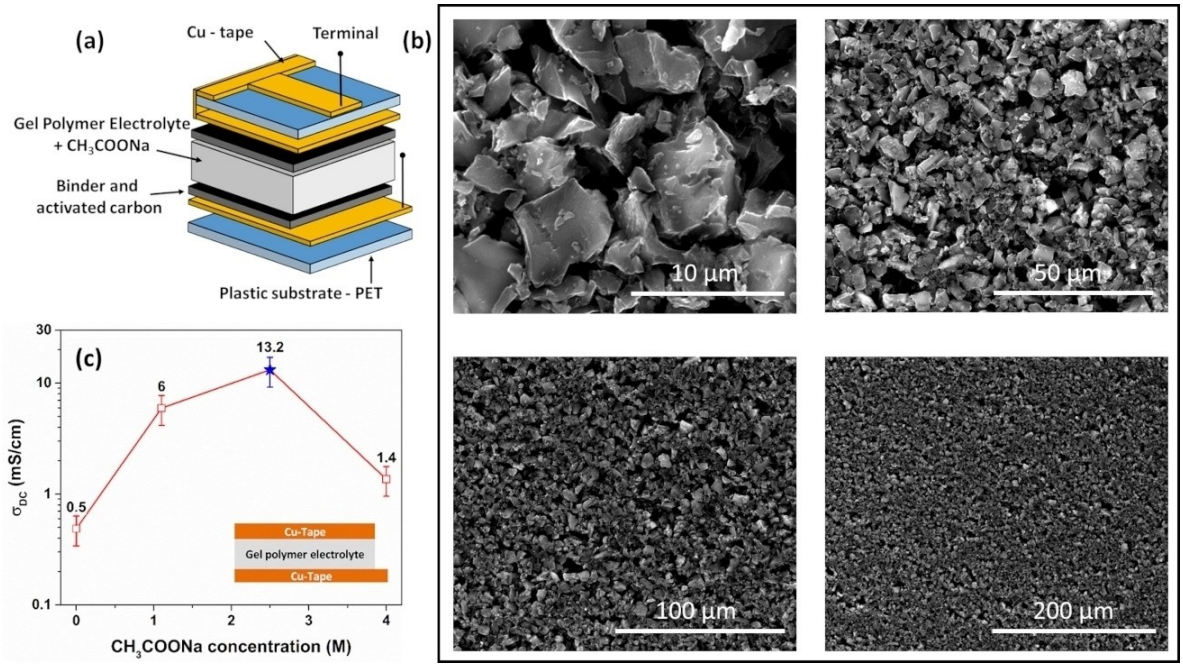


**Figure 1.** (a) Cross-sectional illustration of the symmetric carbon-based supercapacitors fabricated using environmentally friendly materials; (b) SEM images of the surface morphology for the chitosan-based electrode at different scale bar, 10 μm, 50 μm, 100 μm and 200 μm, respectively; (c) Variations in ionic conductivity values at 300 K with respect to the sodium acetate concentration within the hydrogel. The cross-sectional view of the experimental configuration employed for the measurement of electrolyte conductivity is shown in the inset.

when the hydrogel with salt serves as an electrolyte, can be attributed to the lower mobility of the cation ($Na^+$) and anion ($CH_3COO^-$) species within the gel, in comparison to the aqueous electrolyte.[32] A similar decline has also been observed in gel polymer electrolytes containing other salts, such as NaCl.[26] Compared to other anions such as $SO_4^{2-}$ and $Cl^-$, the acetate anion $CH_3COO^-$ possesses a smaller desolvated ionic radius, typically within the range of a few angstroms (e.g. 0.15 nm in water-electrolyte).[30] Consequently, it is anticipated that the acetate anion will readily fit into the majority of pores present in activated carbon, which has an average pore size of 0.85 nm, at the electrode/hydrogel interface.[30,32] This characteristic should enhance the dielectric and long-term stability properties of the proposed symmetric carbon-based supercapacitor.[3]

Figure 2(a) shows the cyclovoltammetry (CV) profiles of symmetric carbon-based supercapacitors, wherein the chitosan is the electrode binder and the hydrogel with a 2.5 M $CH_3COONa$ solution is the gel polymer electrolyte. Here, an almost rectangular shape of the curves, acquired at a low scan rate level ($\nu \leq 50$ mV/s), is observed for the investigated devices. The experimental data corresponding to the CV profiles collected under higher scan rate conditions ($\nu \geq 100$ mV/s) are reported in Figure S2 (a). The formation of a double-layer capacitance at the interface between the electrode and hydrogel is evidenced by the distinct absence of redox peaks.[33] It is important to note that a range of $\pm 1$ V has been chosen as a limiting operation voltage for the SCs, in order to avoid any chemical reactions due to the water decomposition within the GPE.[18]

The gravimetric capacitance $C_S$ (F/g) of the symmetric SC can be calculated by integrating the area under the CV loops using the equation[34]

$$C_S = \frac{1}{m_a \cdot \nu \cdot (V_b - V_a)} \cdot \int_{V_a}^{V_b} i(V)dV. \quad (1)$$

Here, $m_a$ represents the mass of the electrode, $\nu$ is the scan rate, $i(V)$ is the charging/discharging current, $V_b$ and $V_a$ refer to the initial and final potentials, respectively.

Figure 2(b) displays a comparative analysis of the $C_S$ values with respect to various voltage scan rates, spanning from 10 mV/s to 500 mV/s, for the gel polymer containing 2.5 M $CH_3COONa$ and the reference electrolytes employing NaCl as the ionic salt. For all the electrolytes, the computed capacitance values decrease with increasing $\nu$. Here, the highest $C_S$ value, 86.8 F/g at 10 mV/s, is attained by the SC utilizing the hydrogel with 2.5 M of $CH_3COONa$ as the electrolyte. By increasing the scan rate, the $C_S$ value decreases to 34.7 F/g at 500 mV/s, representing a 60% reduction. Compared to the aqueous electrolyte, the utilization of hydrogel increases the capacitance loss as a function of the scan rate, including for the acetate electrolyte. In the case of the aqueous electrolyte with 1 M NaCl, the capacitance loss is only 38%, as indicated in Figure 2(b). However, acetate enhances ion accumulation and pore filling at the electrodes due to the smaller radius of the acetate anion, compared to the SC with GPE + NaCl.

It is important to note that the observed capacitance drop as a function of the scan rate, which is 60% (from 86.8 F/g to 34.7 F/g) for the hydrogel with 2.5 M $CH_3COONa$, is lower than the reduction of 82.6% reported for the gelatin-based electrolyte with NaCl as the salt.[26]

This means that effectively the acetate-based hydrogel positively affects the dielectric response with greater capacitance value and better retention for the SC evaluated. In terms of $C_S$, the capacitance value for the GPE with acetate is consistent with findings reported in the literature for SCs with aqueous electrolytes.[29,30]

In supercapacitors, the storage of charges occurs at the interface between the active material and electrolyte through two distinct processes: faradaic processes involving electron transfer via redox reactions, and non-faradaic processes involv-

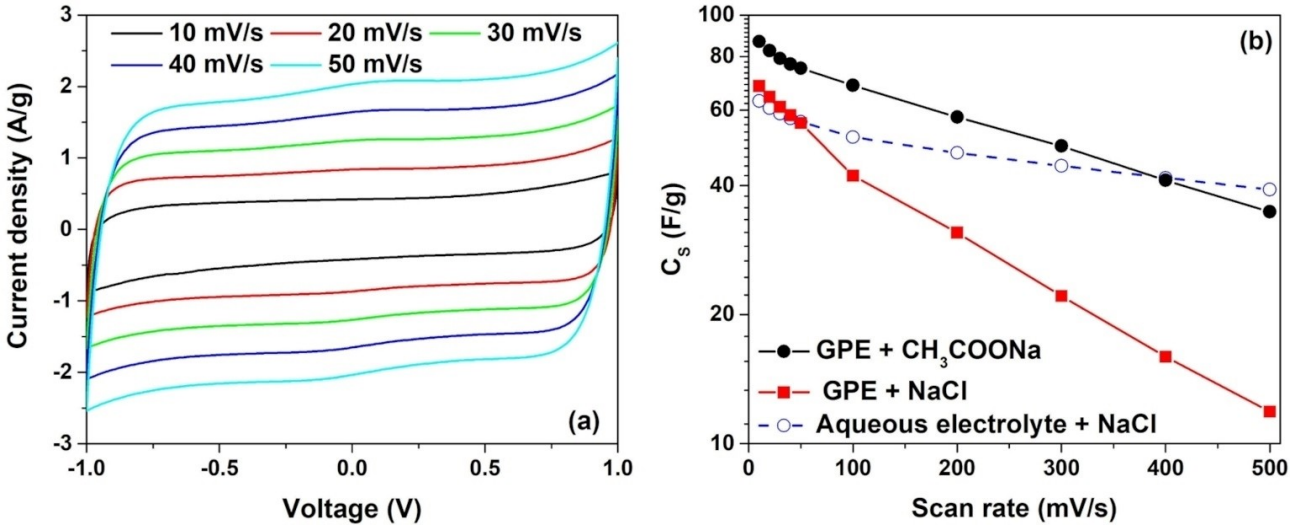


**Figure 2.** (a) Cyclic voltammetry curves of symmetric supercapacitors with gel polymer electrolyte with 2.5 M $CH_3COONa$, acquired within the lower scan rate range ($\nu \leq 50$ mV/s); (b) Comparative evaluation of corresponding gravimetric capacitance values between gel polymer and aqueous-based electrolytes, both utilizing chitosan as the electrode binder.

ing the accumulation of ions at an electrical double-layer. In certain cases, a combination of both mechanisms can be observed.[1] In the latter case, the system exhibits hybrid characteristics, indicating the presence of pseudocapacitive behaviour at the interface between the hydrogel and the porous carbon-based electrode.

Figure 3 illustrates the diffusion-limited (pseudocapacitance) and surface-limited (double-layer capacitance) contributions to the overall capacitance, computed for low scan rate and denoted as $C_S^*$, for the chitosan-based electrode when employing hydrogels and water as the electrolyte. A comprehensive analysis of the current response modelling in supercapacitors, to discern surface and diffusion contributions and their dependence on $\upsilon$, can be found in the supplementary materials. As anticipated, at low scan rate values ($\nu \rightarrow 0$), the total charge is stored through the simultaneous occurrence of faradaic and double-layer charge storage mechanisms at the hydrogel/electrode interfaces. The implementation of the hydrogel as an electrolyte reduces the contribution of the double-layer capacitance compared to supercapacitors fabricated with aqueous electrolytes,[25] as shown in Figure 3. However, in all the devices, the double-layer contribution prevails (over 57.1 %) in the total capacitance, indicating a predominantly capacitive behaviour for the chitosan-based electrode. Specifically, the addition of acetate to the hydrogel enhances the double-layer contribution, approaching a value (67 %), similar to that observed for the aqueous electrolyte (74.2 %). The extracted value of $C_S^*$ is approximately 100 F/g, higher than that measured for the other electrolytes. This finding further demonstrates the increased ion adsorption and pore filling at the electrode/electrolyte interface for the device containing $CH_3COONa$.

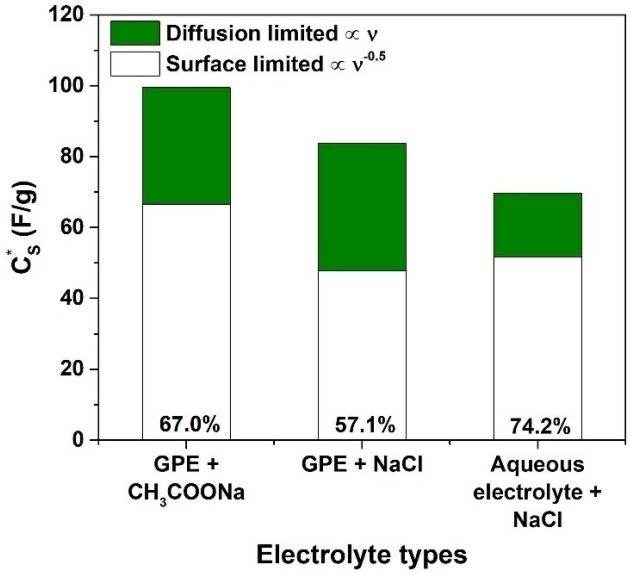


**Figure 3.** Diffusion-limited (pseudocapacitance) and surface-limited (double-layer capacitance) contributions to the overall capacitance $C_S^*$ for the electrolytes investigated: GPE with 2.5 M of sodium acetate, GPE with 2 M NaCl and aqueous electrolyte with 1 M NaCl.

The observed faradaic contribution can be attributed to charge transfer phenomena occurring between functional groups present within chitosan and gelatin, particularly with cationic species such as $Na^+$. In our device, chitosan features hydroxyl (OH) and amine ($NH_2$) functional groups, enhancing the wettability of the carbon electrode surface.[11,16] This enhancement facilitates charge transfer processes and promotes ion adsorption.[11,35,36] Additionally, gelatin contains carboxyl (COOH) and amine ($NH_2$) groups that can interact with the activated carbon at the electrode-electrolyte interface.[11,27] Furthermore, during the denaturation process of native collagen, gelatin may also contain a lower concentration of divalent cations, such as $Ca^{2+}$, $Cu^{2+}$, and $Fe^{2+}$. Numerous studies in the literature have reported interactions between these functional groups (COOH, $NH_2$ and OH) and cationic species, such as $Na^+$ ions originating from the acetate salt present in the electrolyte. These interactions have been shown to initiate redox transitions at the electrode surface.[11,35–37] For example, amine and hydroxyl groups have been observed to induce faradic redox reactions when employed with activated carbon electrodes derived from mango kernels.[36] These charge transfer mechanisms probably contribute to the observed pseudocapacitance behavior depicted in Figure 3.

The galvanostatic charge-discharge (GCD) curves, acquired at various current densities for the chitosan-based supercapacitor with 2.5 M $CH_3COONa$ gel polymer electrolyte, are shown in Figure 4(a). As expected, the dominant capacitive contribution of the double layer result in linear charging and discharging curves. The gravimetric capacitance ($C_S^{GCD}$) extracted from the charge-discharge profiles can be determined by using equation (2), whereas the coulombic efficiency (CE) of the devices can be calculated as the ratio between the charge stored during the charging phase and the charge released during the discharge phase. Furthermore, the equivalent series resistance (ESR) can be evaluated from the voltage drop observed in the GCD profiles by considering equation (3).

Figure 4(b), and (c) display the current dependence of the $C_S^{GCD}$ and CE values, respectively. As can be observed, the $C_S^{GCD}$ values fall within a range consistent with what is reported in Figure 2(b). The CE shows a value of about 90 %, with an increase observed at higher currents, reaching a value of approximately 100 %. These values are consistent with findings reported in the literature for performing devices.[25,26]

In Figure 4(c) the current dependence of the extracted ESR values for all the supercapacitors investigated are shown. Notably, supercapacitors based on hydrogel with acetate, which are characterized by a near-rectangular shape of the CV loop, reveal low series resistance values of about 0.8 Ω. These values are less than one order of magnitude than those documented in the literature for comparable binder materials.[38,39]

It is worth noting that the reference SCs with aqueous and hydrogel electrolytes with NaCl as salt have a value of ESR of 0.25 Ω and 1.0 Ω, respectively. For more details, see Table S1. Figure 5 shows a Ragone plot presenting the specific power versus specific energy for the examined devices. The quantification of energy (*E*) and power (*P*) has been achieved employing equations (4) and (5), respectively. For an effective energy

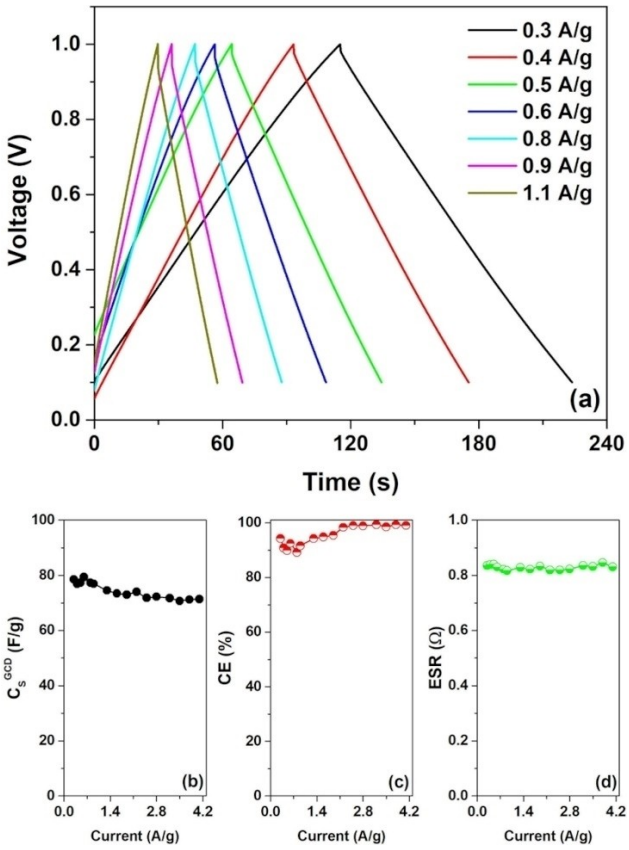


**Figure 4.** (a) Galvanostatic charge and discharge profiles at different current densities for the supercapacitor employing chitosan as the binder with 2.5 M $CH_3COONa$ gel polymer electrolyte; Corresponding current dependence of the extracted (b) gravimetric capacitance, (c) coulombic efficiency, and (d) equivalent series resistance values, respectively.

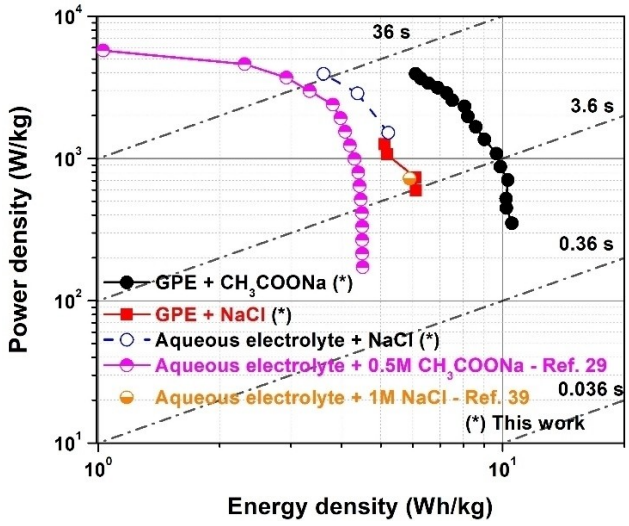


**Figure 5.** Ragone plot for the fabricated devices, compared with other symmetric eco-friendly carbon-based supercapacitors with hydrogel reported in the literature.

performance comparison on the Ragone plot, reference data points have been chosen based on a consistent potential window (0-1 V) and employing the same electrode material properties utilized in the fabrication of the SCs. The SC incorporating chitosan as a binder and the hydrogel doped with acetate salt as a GPE demonstrates superior performance compared to the other investigated devices.

Specifically, the hydrogel-based supercapacitors achieve a peak energy density of 10.6 Wh/kg and a maximum power density of 3940 W/kg. These values are higher than those reported for the same device doped with NaCl based on hydrogel (6.1 Wh/kg and 1256.2 W/kg) and aqueous electrolyte (5.2 Wh/kg and 3925 W/kg) used as reference structures in this study.

To the best of our knowledge, for the acetate-based system the device incorporating 0.5 M of $CH_3COONa$ in an aqueous electrolyte, reported in the literature, exhibits only half the values of energy and power compared to the GPE-based system.[29] Furthermore, Lupo et al. report a value of 5.9 Wh/kg for a potential window of 1 V in an aqueous electrolyte containing 1 M NaCl.[38,39]

The only comparable study reported by Choudhury et al. involves a gelatin-based electrolyte using 3 M NaCl, yielding an energy value of 9.7 Wh/kg. This value is lower than our energy performance shown in Figure 5.[31] Other GPEs based on different polymer hosts,[40–42] such as polyvinyl alcohol (PVA),[43] corn-derived starch[44] and carboxymethylcellulose,[8] have reported lower energy values. For instance, a PVA-based electrolyte, incorporating $H_3PO_4$ and KOH salts, demonstrates a maximum energy value of approximately 4.3 Wh/kg.[43]

## Impedance spectroscopy

To investigate the correlation between dielectric properties, charge storage mechanisms and cycling stability of the supercapacitors for the electrolytes investigated, electrochemical impedance spectroscopy (EIS) measurements have been conducted. This non-invasive technique has been widely utilized in the literature to study energy-related devices, ranging from generation to storage applications.[1,45–47]

The Nyquist plots, reporting the imaginary part, $-Z_{imag}$, as a function of the real part, $Z_{real}$, of the complex impedance, are displayed in Figure 6(a) for supercapacitors with different electrolytes. The spectra obtained for the supercapacitors show a characteristic extended tail at lower frequencies, a common feature observed in the charge storage mechanisms of dielectric materials, along with their associated interfacial phenomena.[1]

Devices exhibiting a purely capacitive behaviour, characterized by ion accumulation without any charge transfer, display a distinct vertical line in impedance spectra. This behaviour can be accurately described by employing a series configuration of resistive and capacitive components. In such a case, the imaginary part of the impedance undergoes a frequency shift approaching the theoretical value of 90°. However, a slight deviation from the ideal response can be observed and it is due to the porous nature of the carbon-based electrode.[1,44,48] Therefore, the dielectric response can be described with a constant phase element (CPE) having phase angles equal to $n{\cdot}90°$, where $n$ ranges from 0 to 1 (practically 0.75 to 1). Here,

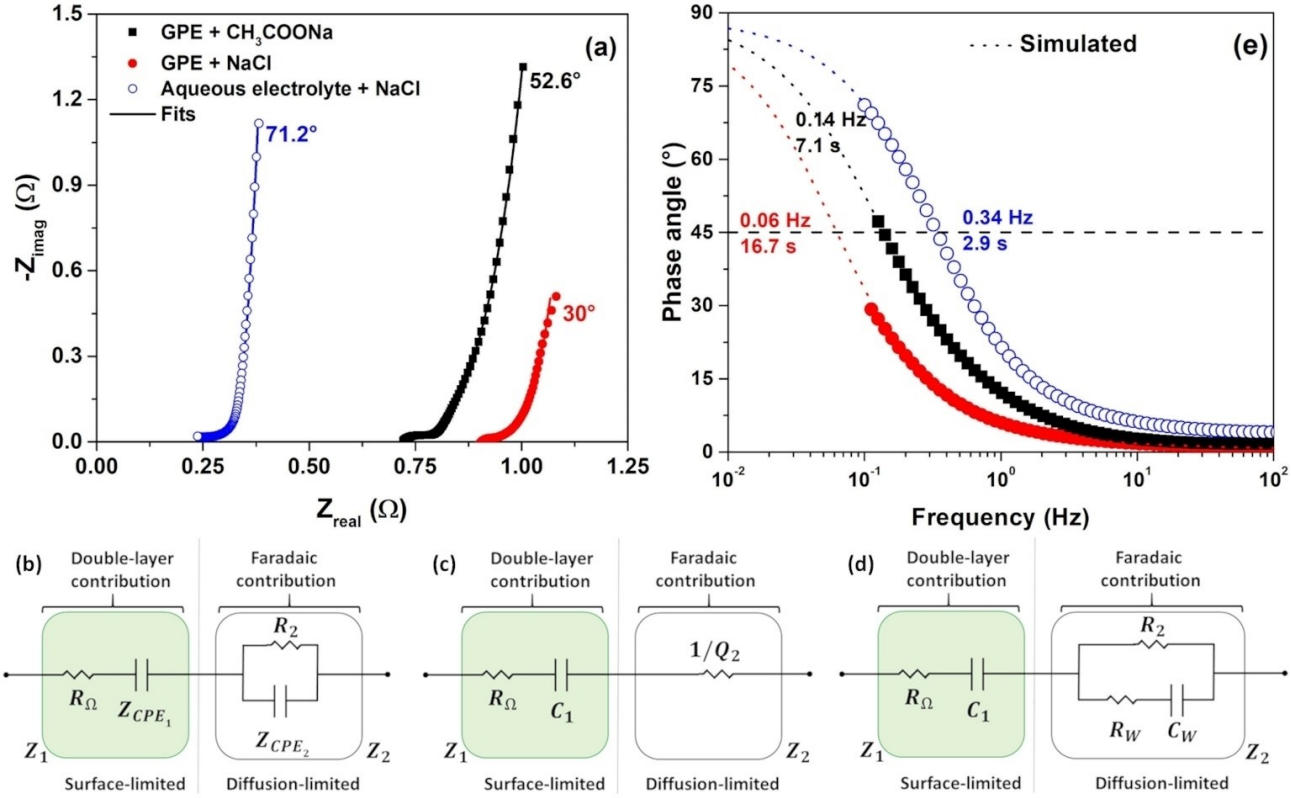


**Figure 6.** (a) Comparison of the impedance spectra and (e) corresponding phase angle as a function of the frequency for supercapacitors with GPE with 2.5 M of sodium acetate, GPE with 2 M NaCl and aqueous electrolyte with 1 M of NaCl, respectively; (b) Equivalent ac circuit used for fitting the impedance spectra of the investigated supercapacitors, (c) simplified versions for a purely capacitive and (d) pseudocapacitance behaviour, respectively. The resultant curves obtained from the fitting procedure, indicated as solid lines, are attained from the equivalent ac circuit. The dotted lines are the corresponding simulated curves at low-frequency region.

the impedance associated with the CPE is $Z_{CPE} = 1/(j\omega)^n Q$. When $n=1$, the CPE is an ideal capacitor, and $Q$ is its capacitance. Otherwise, the CPE deviates from a capacitor and for $n$ close to 0.5 becomes a pure Warburg impedance $Z_W$. The presence of the $Z_W$ suggests the occurrence of faradaic reactions or diffusion processes within the active electrode material and at the interface with the electrolyte.[49] The transport mechanism of the electrolyte within the porous structure manifests as Warburg-type impedances, resulting in a complete capacitive response observed at the lower frequency range.[50,51]

Given that the accumulation of total charge within the system involves the concurrent presence of faradaic and double-layer charge storage mechanisms at the interfaces between the hydrogel and electrodes, the impedance spectra can be effectively represented by a series connection of two distinct contributions, denoted as $Z_1$ and $Z_2$.

$Z_1$ represents the impedance associated with the capacitive/double-layer response, which is modelled as a series combination of a constant phase element ($CPE_1$) and a resistance ($R_\Omega$).[52] On the other hand, $Z_2$ describes the pseudocapacitance/diffusion-limited behaviour, represented by a parallel branch consisting of a constant phase element ($CPE_2$) and the charge-transfer resistance ($R_2$). The ac equivalent circuit employed to model the impedance spectra is illustrated in Figure 6(b). The corresponding fitting curves are displayed in Figure 6(a) as solid lines. The resultant optimal parameters from the fitting process are shown in Table S2.

In this framework, the faradaic contribution modelled with the impedance $Z_2$ exhibits distinct behaviours for the investigated electrolytes. In the case of electrolytes containing NaCl as the salt, the parameter $n_2$ presents values lower than 0.3, and the corresponding CPE impedance transforms into an ohmic contribution $Z_2 \approx 1/Q_2$. Since $1/Q_2$ is significantly smaller than $R_2$, the diffusion contribution of $Z_2$ can be considered negligible. Consequently, the overall impedance is predominantly influenced by the impedance $Z_1$, where $n_1$ approaches 1 indicating a purely capacitive behaviour. The simplified ac equivalent circuit is depicted in Figure 6(c).

Conversely, the presence of sodium acetate in the hydrogel reveals a clear faradaic diffusion process at the porous electrode, characterized by an $n_2$ value of approximately 0.5. As shown in Figure 6(a), an additional slope of the imaginary part of the impedance is observed in the low-frequency region due to the occurrence of faradaic processes at the electrode surface. The resulting faradaic impedance $Z_W$ can be seen as a frequency-dependent resistance, $R_W = \sigma/\omega^{0.5}$, in series with a psuedocapacitance $C_W = 1/(\sigma\omega)^{0.5}$, where $\sigma = Q_2$ represents the Warburg constant. The corresponding simplified ac equivalent circuit is presented in Figure 6(d).

By analyzing the impedance spectra and the corresponding fitting parameters, the models confirm the predominant contribution of double-layer capacitance for all investigated electrolytes, as already shown in Figure 3.

However, the addition of sodium acetate in the hydrogel enhances the faradaic contribution at the porous carbon electrode resulting in a significant increase in overall capacitance.

This further contribution, observed specifically for the GPE + 2.5 M $CH_3COONa$ in Figure 2(b) compared to the other electrolytes, can be attributed to the presence of $C_W$ modelling the presence of pseudocapacitance.

The comparison of phase angle at various frequencies for the investigated SCs is depicted in Figure 6(e). It is a valuable tool for understanding the capacitive characteristics of electrode materials: a phase angle approaching $-45^\circ$ suggests the presence of a pseudocapacitive behaviour.[53]

The relaxation time constant ($\tau_0$) is defined as the shortest time interval necessary for the complete charge or discharge of energy from a device while maintaining an efficiency exceeding 50%.[52] It can be calculated as follows $\tau_0 = (f_0)^{-1}$, where the value of $f_0$ is determined from the phase angle plot at $-45^\circ$.[54] From Figure 6(b), $f_0$ at the phase angle of $-45^\circ$ for the SCs with GPE + sodium acetate and GPE + NaCl are found to be 0.14 Hz and 0.06 Hz and the corresponding $\tau_0$ are about 7.1 s and 16.7 s, respectively. These values are consistent with that found in the literature for the supercapacitor based on activated carbon material.[3]

Although the hydrogel reduces the mobility of the ions, the SC containing sodium acetate shows $\tau_0$ value close to the water-electrolyte, that is 2.9 s.

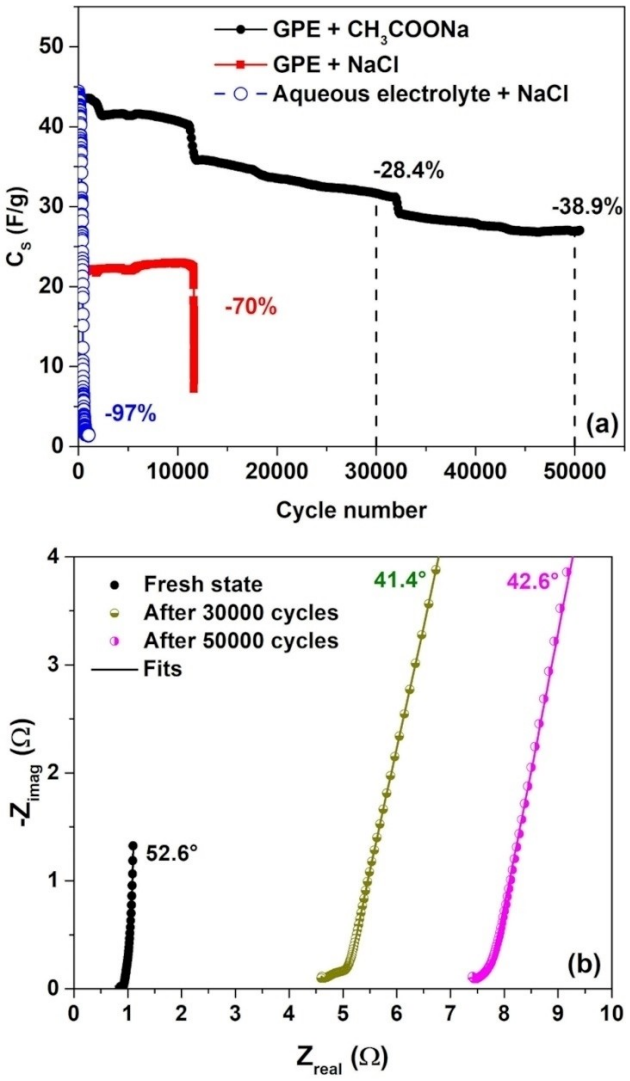


**Figure 7.** (a) Cycle stability of the SC-based GPE carried out with CV cycles at 300 mV/s within the voltage range of 0 to 1 V for the GPE with 2.5 M of sodium acetate, GPE with 2 M NaCl and aqueous electrolyte with 1 M NaCl; (b) Comparison of the impedance spectra during the cycle stability test of the device based on GPE with 2.5 M of sodium acetate. The best-fitting curves, shown as solid lines, are obtained from the ac equivalent circuit in Figure 6(b).

## Cyclability

The endurance of the devices during cycle voltammetry measurements, performed at 300 mV/s within the voltage range of 0 and 1 V, is shown in Figure 7(a). Here, the capacitance values computed for the studied SCs are in agreement with those presented in Figure 2(b). As evidenced, the devices with GPE exhibit more stable dielectric properties compared to the device with aqueous electrolyte (stability below 1000 cycles). In particular, the GPE with NaCl is stable up to 12000 working cycles, whereas the device containing sodium acetate shows extended stability up to 50000 cycles with only a 39% reduction in its initial capacitance value.

This finding exceeds cyclability reported in the literature for SCs based on eco-friendly GPEs.[31,55,56] For instance, only the SCs based on PVA/KOH demonstrate stability within the range of 10000 working cycles.[55] Conversely, devices based on biodegradable polymers obtained from renewable resources (similar to gelatin) as polymer host within the hydrogel (e.g. guar gum) has a lower endurance ($\leq$ 5000 cycles).[56] It is worth noting that the hydrogel incorporating 3 M of NaCl exhibits even lower stability, limited to 1200 cycles.[31] Furthermore, devices utilizing gel polymer electrolytes combined with conducting salts (e.g., $Na_2SO_4$, $Li_2SO_4$, and LiCl) or aqueous electrolytes (e.g., $H_2SO_4$ and KOH) and employing different fillers (such as graphene, $MnO_2$, and carbon nanotubes) within the electrodes, exhibit stability values below 10000 cycles.[32,55,57] It is worth noting that the addition of the $CH_3COONa$ within the hydrogel not only enhances the dielectric properties but also contributes to improved cyclic stability.

To understand the ageing mechanisms during the cycling procedure the impedance spectra have been measured after 30000 and 50000 cycles, respectively. Figure 7(b) shows the comparison of the impedance spectra for the supercapacitor having GPE + 2.5 M $CH_3COONa$ measured during the cycle stability test conducted at 300 mV/s within the voltage range of 0 to 1 V.

The equivalent ac circuit employed to model the impedance spectra is illustrated in Figure 6(b). The corresponding fitting

curves are shown in Figure 7(b) as solid lines. The resulting best-fitting parameters are reported in Table S3. As shown in Figure 7(b), during the cycling procedure the device becomes more resistive. A notable increment of the $R_\Omega$ values (e.g., by one order of magnitude after 50000 cycles), which justifies a shifting of the spectra towards a higher resistance range as a function of the cycle number, has been observed. During extended cycling of the device, various aging phenomena occur within the SC. These processes result in the formation of degradation products that have the potential to obstruct the pores of the electrode or lead to the creation of a passivating layer on the electrode surface. Furthermore, these physical and chemical modifications have a detrimental effect on the charge carrier accumulation at the electrode/electrolyte interface. [20] Nevertheless, the shape of the spectra characterized by a long tail at lower frequencies suggests the persistence of a capacitive contribution. As reported in Table S3, the double-layer contribution modelled with the $CPE_1$ indicates a deviation from ideal capacitor behaviour ($n_1 = 1$) with a decrease in the $n_1$ parameter to 0.75. This decrease explains the decline in the phase angle at a lower frequency range. Here, the contribution of the pseudocapacitance is strongly reduced, as evidenced by the significant drop in the $Q_2$ parameter. This reduction as a function with the cycles explains the four distinct descent steps in Figure 7(a). Consequently, the cycling test shows that the supercapacitor with GPE and sodium acetate as salt possesses long stability (up to 50000 cycles) with capacitance retention (ca. 61%) that can primarily be attributed to the double-layer component. This value is consistent with what has been reported in Figure 3 from the estimation of the double-layer contribution (ca. 67%) to the overall capacitance $C_S^*$ for the GPE with acetate. It should be noted that the capacitance loss, related solely to the double-layer contribution, is only 6%.

Figure 8(a) report a comparative analysis of the cycle stability, energy and dielectric performance of the investigated SCs. These devices have been fabricated by using different electrolyte types and employing chitosan as the electrode binder material. While aqueous electrolytes possess superior characteristics in terms of ionic conductivity, interfacial wettability, safety, and environmental friendliness,[32] the experimental data indicate that the incorporation of a hydrogel boosts the stability of the ultimate device, thereby extending operational lifespan of up to 50000 cycles (e.g., GPE + acetate). Moreover, the addition of acetate as a salt additive improves the specific energy density to 10.6 kWh/kg with a value of internal resistance lower than 1 Ω.

Despite the increase of the internal resistance associated with the gel polymer electrolyte and higher $\tau_0$, the dielectric properties stay unaffected compared to aqueous electrolytes.

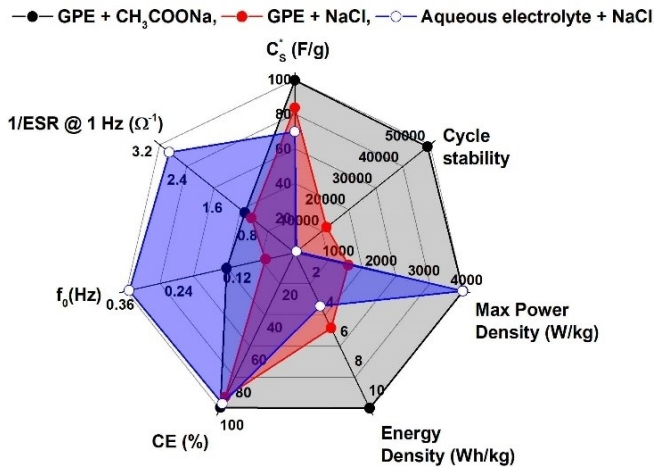


**Figure 8.** Radar plot comparing the dielectric properties of the supercapacitors utilizing GPE with 2.5 M of sodium acetate, GPE with 2 M NaCl and 1 M of NaCl in aqueous electrolytes with chitosan as an electrode binder, respectively.

## Conclusions

A hydrogel composed on gelatin and incorporating 2.5 M of $CH_3COONa$ has been utilized as a gel polymer electrolyte in symmetric carbon-based supercapacitors, with chitosan serving as a sustainable binder in the electrode. To assess the influence of sodium acetate on the device performance, a comparison analysis with reference structures based on aqueous and gel-based electrolytes with NaCl has been made. The most efficient supercapacitors, utilizing sodium acetate and hydrogel, exhibit a gravimetric capacitance value of approximately 100 F/g, a series resistance of 0.8 Ω, and higher coulombic efficiency.

The electrode interface experiences both faradaic and double-layer mechanisms of charge storage. The presence of acetate enhances the double-layer component, which becomes the predominant charge storage mechanism at the electrode/electrolyte interface. Moreover, the increased ion adsorption and pore filling at the electrode/electrolyte interface diminishes the loss of capacitance as a function of the scan rate. Impedance spectra modelling further confirms the roles of both charge storage mechanisms and provides evidence of pseudocapacitance.

In terms of cyclability, the addition of acetate increases cycle life enabling the supercapacitors to endure up to 50000 cycles, surpassing the performance of hydrogel with NaCl (12000 cycles). After prolonged cycling, the modelling of the impedance spectra indicates increased device resistance and a substantial reduction in the pseudocapacitance contribution. Only the double layer contribution remains with a value of about 30 F/g after 50000 cycles, corresponding to a retention of 61% from its initial uncycled value. Notably, the capacitance loss, related solely to the double-layer contribution, is only 6%. Here, the best-performing device delivers about 10.6 Wh/kg of energy at a high-power density of 3940 W/kg.

These findings highlight the significant impact of sodium acetate on the electrochemical performance of supercapacitors, emphasizing its potential for improving the energy storage capabilities of sustainable devices.

## Experimental Section

### Materials preparation

Test structures for supercapacitors were manufactured on polyethylene terephthalate (PET) foils (Melinex ST 504, DuPont Teijin Films, Chester, VA, USA, thickness 125 μm) that were coated with copper (Cu) tape (Kohree, City of Industry, CA, USA, thickness 40 μm). Henkel Electrodag PF407 C graphite ink was deposited onto the PET/Cu substrates using blade coating (Proceq ZAA 2300, Zehntner GmbH Testing Instruments, Sissach, Switzerland), followed by thermal annealing at 90 °C for 30 minutes. This results in 50 μm thick films. The electrode active material was formulated by dissolving activated carbon (Kuraray YP 80F, Tokyo, Japan, with characteristic $V_{micro} < 2$ nm = 0.652 $cm^3/g$ and specific surface area (SSA) = 2093 $m^2 g^{-1}$) derived from coconut shells, along with a binder, in ultrapure water (Milli-Q), following the composition of 95 : 5 wt.%. The binder under investigation is chitosan (Sigma-Aldrich, chitosan from shrimp shells, Saint Louis, MO, USA), which necessitated an acidic solution for dissolution. Therefore, acetic acid was incorporated into the formulation. The AC/binder mixture was stirred until a uniform carbonaceous slurry was achieved. Subsequently, the slurry was applied onto the PET–Cu - Graphite stack through blade coating and allowed to air dry at room temperature. During this phase, the electrodes were weighed to ascertain the AC mass loading $m_a$, which ranged from 6 to 6.8 mg/$cm^2$. A total of 15 samples were prepared and the electrodes were paired up based on similar mass for the supercapacitor devices.

The gel polymer electrolyte was formulated by mixing 2 g of gelatin (Sigma-Aldrich, gelatin from porcine skin) with 15 ml of a 2.5 M $CH_3COONa$ aqueous solution, aiming to achieve optimal gel electrolyte conductivity. Subsequently, 1.5 ml of glycerol was introduced into the solution while stirring at 65 °C until the complete dissolution of the gelatin powder was achieved. In order to reduce intermolecular forces in the gelatin network, glycerol was added as a plasticizer. This increases the mobility of polymeric chains and improves film flexibility.[58] Hydrogels with different molar salt concentrations were fabricated using 0 M, 1 M, 2.5 M and 4 M of sodium acetate aqueous solutions. The supercapacitor was completed by sandwiching another electrode to form a structure. The electrode area $A$ was 2.5×4 $cm^2$.

### Morphology characterization

The morphology of the sample was investigated by a Field Emission SEM (FeSEM), model INSPECT F from FEI. The FeSEM images were acquired by using a secondary electrons (SE) detector with an acceleration voltage of 30 kV, a working distance of 15 mm, and a nominal resolution of 1.3 nm at 20 kV.

Samples observation without any preparation, except for the electrical grounding of the surface, was allowed by the high conductive nature of the graphite-based material.

### Electrochemical characterization

The electrochemical analyses, including cyclic voltammetry, galvanostatic charge-discharge, and electrochemical impedance spectroscopy, were conducted using a commercial platform (Arkeo - Cicci Research) at ambient temperature. The measurements were performed in a two-electrode configuration, utilizing supercapacitor devices with an average area of approximately 10 $cm^2$. Electrochemical impedance spectroscopy measurements were performed across a frequency range from 100 mHz to 10 kHz, employing an alternating signal with an amplitude of 50 mV at the open-circuit voltage.

The galvanostatic discharge curves were used to determine the specific capacitances of the symmetric supercapacitors, through the following equation[28]

$$C_S^{GCD} = \frac{I_D \cdot \Delta t}{m_a \cdot \Delta V}, \tag{2}$$

where $\Delta t$, $\Delta V$ and $I_D$ represent the interval for full discharge, the operating potential difference of a SC and the discharge current, respectively.

The equivalent series resistance can be estimated by[34]

$$ESR = \frac{IR_{drop}}{2 \cdot I_D}, \tag{3}$$

where $IR_{drop}$ signifies the voltage drop between the initial two points of the discharge plot.

The energy $E$ (Wh/Kg) and the power $P$ (W/Kg) densities of supercapacitors were calculated by considering the following equations[34]

$$E = \frac{1}{2} \cdot C_S^{GCD} \cdot (\Delta V)^2 = \frac{1}{2} \cdot C_S^{GCD} \cdot \frac{\left(V_{max} - V_{min} - IR_{drop}\right)^2}{3.6}, \tag{4}$$

and

$$P = \frac{E}{t_{disc}} \cdot 3600, \tag{5}$$

where $V_{max}$ and $V_{min}$ refer to the maximum and minimum applied voltage to the device, respectively, while $t_{disc}$ represents the corresponding discharge period.

## Supporting Information

The authors have cited additional references within the Supporting Information.[27,59–61]

The data that support the findings of this study are available from the corresponding author upon reasonable request. ((Data Availability and Conflicts of Interest statements are generated automatically from information in Editorial Manager!))

## Acknowledgements

This research was funded in the Program Agreement between the Italian National Agency for New Technologies, Energy and Sustainable Economic Development (ENEA) and the Ministry of Environment and Energy Safety for Electric System Research, in the framework of its Implementation Plan for 2022–2024. In particular, the activity is included in Project 1.5 "High-efficiency buildings for the energy transition", Work Package 3 "Innovative technologies and components for increasing the energy performance of buildings". C. Barone and S. Pagano gratefully acknowledge the financial support from University of Salerno

through Projects nr. FRB20BARON, FRB21CAVAL, FRB22PAGAN, and FRB23BARON.

## Conflict of Interests

The authors declare no conflict of interest.

## Data Availability Statement

The data that support the findings of this study are available from the corresponding author upon reasonable request.

**Keywords:** Charge storage mechanisms · Cyclic voltammetry · Gel-polymer electrolyte · Sodium acetate · Sustainable Chemistry

[1] T. S. Mathis, N. Kurra, X. Wang, D. Pinto, P. Simon, Y. Gogotsi, *Adv. Energy Mater.* **2019**, *9*, 1902007.
[2] A. Noori, M. F. El-Kady, M. S. Rahmanifar, R. B. Kaner, M. F. Mousavi, *Chem. Soc. Rev.* **2019**, *48*, 1272.
[3] P. Simon, Y. Gogotsi, *Nat. Mater.* **2020**, *19*, 1151.
[4] A. H. Mohd Aman, N. Shaari, R. Ibrahim, *Int. J. Energy Res.* **2021**, *45*, 8389.
[5] G. Landi, H.-C. Neitzert, *ACS Appl. Electron. Mater.* **2021**, *3*, 2790.
[6] X. Aeby, A. Poulin, G. Siqueira, M. K. Hausmann, G. Nyström, *Adv. Mater.* **2021**, *33*, 2101328.
[7] S. C. Teixeira, N. O. Gomes, T. V. de Oliveira, P. Fortes-Da-Silva, N. de F. F. Soares, P. A. Raymundo-Pereira, *Biosens. Bioelectron. X* **2023**, *14*, 100371.
[8] K. Fic, A. Platek, J. Piwek, E. Frackowiak, *Mater. Today* **2018**, *21*, 437.
[9] B. Modarress Fathi, A. Ansari, A. Ansari, *Sustainability* **2022**, *14*, 10161.
[10] Y. Hu, J. Ouyang, W. Xiong, R. Wang, Y. Lu, W. Yin, Y. Fan, Z. Li, K. Du, X. Li, Y. Luo, *J. Colloid Interface Sci.* **2023**, *648*, 674.
[11] D. Bresser, D. Buchholz, A. Moretti, A. Varzi, S. Passerini, *Energy Environ. Sci.* **2018**, *11*, 3096.
[12] A. Cholewinski, P. Si, M. Uceda, M. Pope, B. Zhao, *Polymers (Basel).* **2021**, *13*, 631.
[13] E. S. Appiah, P. Dzikunu, N. Mahadeen, D. N. Ampong, K. Mensah-Darkwa, A. Kumar, R. K. Gupta, M. Adom-Asamoah, *Molecules* **2022**, *27*, DOI 10.3390/molecules27196556.
[14] K. Murashko, D. Nevstrueva, A. Pihlajamäki, T. Koiranen, J. Pyrhönen, *Energy* **2017**, *119*, 435.
[15] P. Ruschhaupt, A. Varzi, S. Passerini, *ChemSusChem* **2020**, *13*, 763.
[16] L. Bargnesi, A. Rozzarin, G. Lacarbonara, S. Tombolesi, C. Arbizzani, *ChemElectroChem* **2023**, *10*, 1.
[17] S. M. Abu, M. N. M. Ansari, A. Q. Al-Shetwi, K. M. Muttaqi, M. A. Hannan, *IEEE Trans. Ind. Appl.* **2023**, *59*, 3133.
[18] X. Zang, C. Shen, M. Sanghadasa, L. Lin, *ChemElectroChem* **2019**, *6*, 976.
[19] A. Lewandowski, A. Olejniczak, M. Galinski, I. Stepniak, *J. Power Sources* **2010**, *195*, 5814.
[20] E. Pameté, L. Köps, F. A. Kreth, S. Pohlmann, A. Varzi, T. Brousse, A. Balducci, V. Presser, *Adv. Energy Mater.* **2023**, *2301008*, DOI 10.1002/aenm.202301008.
[21] X. Cheng, J. Pan, Y. Zhao, M. Liao, H. Peng, *Adv. Energy Mater.* **2018**, *8*, 1702184.
[22] M. Zhu, L. Yu, S. He, H. Hong, J. Liu, L. Gan, M. Long, *ACS Appl. Energ. Mater.* **2019**, *2*, 5992.
[23] S. Bashir, M. Hina, J. Iqbal, A. H. Rajpar, M. A. Mujtaba, N. A. Alghamdi, S. Wageh, K. Ramesh, S. Ramesh, *Polymers (Basel).* **2020**, *12*, 1.
[24] I. Babeli, G. Ruano, A. Puiggalí-Jou, M. Ginebra, C. Alemán, J. Garcia-Torres, *Adv. Sustainable Syst.* **2021**, *5*, 2000273.
[25] G. Landi, L. La Notte, A. L. Palma, A. Sorrentino, M. G. Maglione, G. Puglisi, *Nanomaterials* **2021**, *12*, 46.
[26] G. Landi, L. La Notte, A. L. Palma, G. Puglisi, *Polymers (Basel).* **2022**, *14*, 4445.
[27] G. Landi, V. Granata, R. Germano, S. Pagano, C. Barone, *Nanomaterials* **2022**, *12*, 2227.
[28] G. Landi, A. Sorrentino, S. Iannace, H. C. Neitzert, *Nanotechnology* **2017**, *28*, 054005.
[29] J. Piwek, A. Platek, K. Fic, E. Frackowiak, *Electrochim. Acta* **2016**, *215*, 179.
[30] B. Dyatkin, V. Presser, M. Heon, M. R. Lukatskaya, M. Beidaghi, Y. Gogotsi, *ChemSusChem* **2013**, *6*, 2269.
[31] N. A. Choudhury, S. Sampath, A. K. Shukla, *J. Electrochem. Soc.* **2008**, *155*, A74.
[32] B. Pal, S. Yang, S. Ramesh, V. Thangadurai, R. Jose, *Nanoscale Adv.* **2019**, *1*, 3807.
[33] Y. Zhu, S. Murali, M. D. Stoller, K. J. Ganesh, W. Cai, P. J. Ferreira, A. Pirkle, R. M. Wallace, K. A. Cychosz, M. Thommes, D. Su, E. A. Stach, R. S. Ruoff, *Science* **2011**, *332*, 1537.
[34] T. Esawy, M. Khairy, A. Hany, M. A. Mousa, *Appl. Phys. A* **2018**, *124*, 566.
[35] M. Rajkumar, C. T. Hsu, T. H. Wu, M. G. Chen, C. C. Hu, *Prog. Nat. Sci. Mater. Int.* **2015**, *25*, 527.
[36] D. Jain, J. Kanungo, S. K. Tripathi, *Mater. Chem. Phys.* **2019**, *229*, 66.
[37] Y. Shu, Q. Bai, G. Fu, Q. Xiong, C. Li, H. Ding, Y. Shen, H. Uyama, *Carbohydr. Polym.* **2020**, *227*, 115346.
[38] S. Lehtimäki, A. Railanmaa, J. Keskinen, M. Kujala, S. Tuukkanen, D. Lupo, *Sci. Rep.* **2017**, *7*, 46001.
[39] J. Keskinen, A. Railanmaa, D. Lupo, *J. Energy Storage* **2018**, *16*, 243.
[40] W. Li, X. Li, X. Zhang, J. Wu, X. Tian, M. J. Zeng, J. Qu, Z. Z. Yu, *ACS Appl. Energ. Mater.* **2020**, *3*, 9408.
[41] C. Liu, H. Wu, X. Wang, J. Fan, H. Su, D. Yang, Y. Wei, F. Du, Y. Dall'Agnese, Y. Gao, *Energy Storage Mater.* **2023**, *54*, 164.
[42] T. Xu, D. Yang, S. Zhang, T. Zhao, M. Zhang, Z.-Z. Yu, *Carbon* **2021**, *171*, 201.
[43] R. Zhang, X. Jing, Y. Chu, L. Wang, W. Kang, D. Wei, H. Li, S. Xiong, *J. Mater. Chem. A* **2018**, *6*, 17730.
[44] M. F. Shukur, R. Ithnin, M. F. Z. Kadir, *Electrochim. Acta* **2014**, *136*, 204.
[45] S. Vijaya, G. Landi, J. J. Wu, S. Anandan, *J. Power Sources* **2020**, *478*, 229068.
[46] V. Subbiah, G. Landi, J. J. Wu, S. Anandan, *Phys. Chem. Chem. Phys.* **2019**, *21*, 25474.
[47] J. Bisquert, G. Garcia-Belmonte, P. Bueno, E. Longo, L. O. Bulhões, *J. Electroanal. Chem.* **1998**, *452*, 229.
[48] R. Di Giacomo, B. Maresca, M. Angelillo, G. Landi, A. Leone, M. C. Vaccaro, C. Boit, A. Porta, H. C. Neitzert, *IEEE Trans. Nanotechnol.* **2013**, *12*, 1026.
[49] G. Landi, A. Sorrentino, F. Fedi, H. C. Neitzert, S. Iannace, *Nano Energy* **2015**, *17*, 348.
[50] A. A. Moya, *J. Power Sources* **2018**, *397*, 124.
[51] J. Huang, Y. Gao, J. Luo, S. Wang, C. Li, S. Chen, J. Zhang, *J. Electrochem. Soc.* **2020**, *167*, 166503.
[52] W. W. Liu, Y. Q. Feng, X. Bin Yan, J. T. Chen, Q. J. Xue, *Adv. Funct. Mater.* **2013**, *23*, 4111.
[53] V. K. Mariappan, K. Krishnamoorthy, P. Pazhamalai, S. Sahoo, S. J. Kim, *Electrochim. Acta* **2018**, *265*, 514.
[54] M. Kroupa, G. J. Offer, J. Kosek, *J. Electrochem. Soc.* **2016**, *163*, A2475.
[55] A. Dutta, J. Mahanta, T. Banerjee, *Adv. Sustainable Syst.* **2020**, *4*, 1.
[56] Y. N. Sudhakar, M. Selvakumar, D. K. Bhat, *Mater. Sci. Eng. B* **2014**, *180*, 12.
[57] T. Xu, K. Liu, N. Sheng, M. Zhang, W. Liu, H. Liu, L. Dai, X. Zhang, C. Si, H. Du, K. Zhang, *Energy Storage Mater.* **2022**, *48*, 244.
[58] S. Rivero, M. A. García, A. Pinotti, *Innovative Food Sci. Emerging Technol.* **2010**, *11*, 369.
[59] S. Ardizzone, G. Fregonara, S. Trasatti, *Electrochim. Acta* **1990**, *35*, 263.
[60] J. Wang, J. Polleux, J. Lim, B. Dunn, *J. Phys. Chem. C* **2007**, *111*, 14925.
[61] K. B. Hatzell, M. Beidaghi, J. W. Campos, C. R. Dennison, E. C. Kumbur, Y. Gogotsi, *Electrochim. Acta* **2013**, *111*, 888.

Manuscript received: August 31, 2023
Revised manuscript received: October 10, 2023
Version of record online: November 6, 2023